HSPI The Open Access Publisher

J R O JOURNAL OF RADIOLOGY AND ONCOLOGY
ISSN 2573-7724

Research Article

Comprehensive Acceptance Testing and Performance Evaluation of the Symbia Intevo Bold SPECT/CT System for Clinical Use

Subhash Chand Kheruka*, Naema Al-Maymani, Noura Al-Makhmari, Huda Al-Saidi, Sana Al-Rashdi, Anas Al-Balushi, Anjali Jain, Khulood Al-Riyami and Rashid Al-Sukaiti

Department of Radiology & Nuclear Medicine, Sultan Qaboos Comprehensive Cancer Care, and Research Center (University Medical City), Muscat, Oman

Abstract

Aim: This prospective study reports the acceptance testing of the Symbia Intevo Bold SPECT/CT scanner (Siemens Healthineers), recently installed at SQCCCRC, University Medical City, Muscat, Oman, before its clinical implementation.

Materials and methods: The acceptance tests were performed using a Low Energy High Resolution (LEHR) collimator and Technetium-99m (Tc-99m) as the radioactive source, following the manufacturer's protocols. The tests included physical inspection, peaking and tuning, intrinsic and extrinsic uniformity calibration, intrinsic energy resolution, and planar spatial resolution without scatter. Key performance parameters such as full-width at half-maximum (FWHM), system sensitivity, and count rate performance were evaluated.

Results: All critical acceptance tests, including intrinsic energy resolution, energy calibration (symmetric curve), and extrinsic uniformity with the LEHR collimator, were completed and met the required specifications. System sensitivity and count rate performance were within the expected ranges, confirming the system's readiness for clinical use.

Conclusion: The Symbia Intevo Bold SPECT/CT system passed all performance tests successfully. The acceptance testing validated the system's optimal performance following international standards, ensuring its suitability for clinical operations.

More Information

***Address for correspondences:** Subhash Chand Kheruka, Department of Radiology & Nuclear Medicine, Sultan Qaboos Comprehensive Cancer Care, and Research Center (University Medical City), Muscat, Oman, Email: skheruka@gmail.com

Submitted: February 13, 2025
Approved: February 18, 2025
Published: February 19, 2025

How to cite this article: Kheruka SC, Al-Maymani N, Al-Makhmari N, Al-Saidi H, Al-Rashdi S, Al-Balushi A, et al. Comprehensive Acceptance Testing and Performance Evaluation of the Symbia Intevo Bold SPECT/CT System for Clinical Use. J Radiol Oncol. 2025; 9(1): 017-030. Available from: https://dx.doi.org/10.29328/journal.jro.1001076

Keywords: Symbia intevo bold; Tc-99m; LEHR collimator; Acceptance testing; SPECT/CT; Spatial resolution; System sensitivity

Introduction

The gamma camera is among the most widely utilized instruments in nuclear medicine for evaluating physiological function and diagnosing a range of pathologies. It plays a crucial role in imaging the bio-distribution of radiopharmaceuticals through dynamic and static studies of biological tissues [1,2]. This technology enables healthcare providers to capture functional images by detecting gamma radiation emitted from radiotracers, making it highly effective in identifying abnormalities such as cancer, cardiovascular diseases, and skeletal disorders.

One of the significant strengths of gamma cameras lies in their ability to integrate functional imaging with anatomical details obtained from X-ray or CT scans. This fusion of imaging modalities provides a comprehensive view of the patient's condition [3]. For instance, single-photon emission computed tomography (SPECT), an enhancement of gamma camera functionality, enables precise three-dimensional localization of diseases, leading to more accurate diagnoses [4].

The recent installation of the Symbia Intevo Bold SPECT/CT system at the Sultan Qaboos Comprehensive Cancer Care & Research Center (SQCCCRC) signifies a major milestone in the advancement of nuclear medicine in Oman. This achievement underscores the region's commitment to improving diagnostic capabilities and integrating cutting-edge technology into its healthcare infrastructure.

The performance of gamma cameras, however, can vary

based on several factors, including the type of detector crystal used. The most commonly utilized materials for these detectors are hygroscopic Sodium Iodide (NaI) crystals, though newer technologies such as Cadmium-Zinc-Telluride (CZT) crystals offer improved performance [5,6]. Environmental conditions, such as temperature and humidity, can also significantly impact the functionality of gamma cameras [7]. Therefore, ensuring consistent image quality and minimizing patient radiation exposure necessitates rigorous quality assurance, including regular calibration and performance evaluations [8,9].

Acceptance testing forms a vital component of this quality assurance process. It provides baseline performance data to confirm that the equipment meets safety standards, performance benchmarks, and manufacturer specifications [10-12]. Routine acceptance tests for dual-head SPECT gamma cameras typically include evaluations of planar and rotational uniformity, spatial resolution, and the Center of Rotation (COR)—all of which are essential for maintaining image quality and diagnostic accuracy [13,14]. Previous studies have extensively documented the protocols and benefits of gamma camera acceptance testing [15,16].

By assessing critical parameters such as uniformity, resolution, and sensitivity, gamma cameras continue to serve as indispensable tools in nuclear medicine, delivering high-quality diagnostic images that support effective patient care and treatment planning [17-21].

Materials and methods

The Dual-Head SPECT Gamma Camera (Symbia Intevo Bold), equipped with a standard 3/8" thick NaI crystal head, was installed and commissioned at the Sultan Qaboos Comprehensive Cancer Care & Research Centre (SQCCCRC). The gamma camera has a detector of 53.3 × 38.7 cm, ensuring superior image quality and extensive coverage for various diagnostic requirements [1,2]. The system was designed to operate within an energy range of 35 to 588 keV, making it suitable for various applications in nuclear medicine. Multiple acquisition modalities were evaluated to ascertain the system's capacity to provide an extensive array of diagnostic functionalities [3,4]. Quantitative accuracy evaluations indicated that the imaging outcomes were exact, with a variance of less than 5%. All testing was performed in compliance with NEMA requirements (NEMA NU 1-2012) [5]. A Low Energy High Resolution (LEHR) collimator was used to assess the image performance. The uniformity test with Tc-99m and Co-57 was conducted to evaluate the detector's constant response over the whole field of view, hence minimising artefacts and enhancing reliability [6]. The spatial resolution assessment was conducted to evaluate the system's ability to differentiate tiny structures, using full width at half-maximum (FWHM) measurements of point sources. The sensitivity assessment was conducted to evaluate the system's efficacy in detecting gamma radiation, guaranteeing optimal photon capture from Tc-99m, hence enhancing patient dose control and picture quality [9]. The evaluation of energy resolution ascertained the system's capacity to distinguish between distinct photon energies, minimising scatter and improving picture quality [10,11]. Linearity testing was performed to verify that spatial precision was maintained over the whole detector, guaranteeing a distortion-free image [12,13]. All tests were conducted using the appropriate collimator, validating the system's capacity to generate high-resolution diagnostic pictures. Upon the conclusion of acceptance testing, all surfaces, including tables and stands, were decontaminated. Furthermore, motion and axial calibrations of the gamma camera were executed, followed by energy calibration and automated detector adjustment [14]. Acceptance testing and annual surveys for Dual-Head SPECT Gamma Camera systems must thoroughly inspect the system's physical condition, shielding integrity, safety interlocks, and the basic functionality of its associated computers and monitors. It is crucial to document all findings in a comprehensive report.

Physical inspection

Equipment condition assessment: A detailed physical inspection of the camera and all related components was performed. The inspection focused on identifying any visible defects such as scratches, cracks, or loose parts that might compromise system functionality. All filters were checked to ensure they were free of clogs or leaks, which could affect the imaging quality or system safety. The external surfaces of the camera were inspected for cleanliness and the absence of contamination.

Collimator mounting and integrity: The installed Low Energy High Resolution (LEHR) collimators were thoroughly examined to verify they were correctly mounted and securely fastened. This included ensuring that the collimators could be easily switched when necessary. Proper alignment and mechanical integrity of the collimators are essential for ensuring that the imaging system maintains its precision and does not produce artifacts or distortions.

Detector movement and table functionality: The detector movement and table motion were tested to ensure smooth operation without any abnormal sounds, hesitations, or mechanical issues. The axial movement of the camera and table was observed to ensure accurate positioning during patient scans. Proper movement of these components is critical to obtaining clear, artifact-free images during both static and dynamic studies.

Control panel and positioning lights: The functionality of the control panel and the light markers, which guide patient positioning, were tested. All switches and indicators were verified to be responsive and operational. This ensures that operators can accurately position patients and perform diagnostic procedures without errors related to improper system function.

Safety systems and interlocks

Emergency stop and collision sensors: Safety systems, including emergency stop buttons and collision sensors, were rigorously tested to ensure that they function correctly. The emergency stop buttons, when pressed, should immediately halt all camera operations, safeguarding both the patient and the operator in the event of a malfunction. Additionally, collision sensors, particularly those on movable components such as the collimator, were tested to detect any contact and stop motion automatically, preventing potential injuries or equipment damage.

Radiation and room safety checks: Radiation warning lights and other room safety indicators were checked for visibility and functionality. These lights alert staff to radiation use, ensuring that proper protective measures are taken. Warning signs were inspected to verify that they were clearly displayed and appropriately located. The room door closure was tested to ensure it properly seals the room during imaging, maintaining a controlled environment and minimizing radiation exposure to those outside.

Personal protective devices: The availability and condition of personal protective devices, such as lead aprons, were verified. These devices are critical for protecting operators from radiation exposure during gamma camera procedures. The operator's ability to view the patient from the control room window was also confirmed, ensuring unobstructed supervision during scans.

Shielding integrity and radiation protection

Detector shielding inspection: An important part of the installation process involved testing the shielding integrity of the detector. Following NEMA guidelines, a leak scan was performed around the detector using a small radionuclide source (~1 mCi of 99mTc). This test involved moving the source around the detector and observing the count rates to identify any potential radiation leaks. Special attention was paid to the collimator interface to ensure that there were no radiation escapes at the point where the collimator meets the detector. Proper shielding is essential for both patient and operator safety.

Camera shielding and safety: The overall camera shielding was inspected to detect any potential weak points or damage that could lead to radiation leakage. Maintaining the integrity of the camera's shielding ensures that no unintended radiation exposure occurs, providing a safe environment for patients and healthcare workers. Any shielding defects were identified and scheduled for immediate correction.

System functionality and calibration

Image header information: The system's ability to correctly capture and display patient information within the image headers was verified. This includes details such as patient identification, date, and time of the scan. Accurate recording of this information is critical for proper patient record-keeping and traceability in diagnostic procedures.

Motion and axial calibration: The calibration of the camera's motion and axial alignment was performed to ensure that the system could move smoothly and accurately during imaging. This process helps confirm that the gamma camera can maintain precise positioning throughout the scan, ensuring the integrity of both static and dynamic images. Additionally, energy calibration was carried out to fine-tune the camera's energy detection settings, ensuring accurate and consistent imaging results.

Intrinsic and extrinsic calibration and verification

Preparation of the Tc-99m point source: To carry out intrinsic calibration and verification for the gamma camera, we prepared a Tc-99m point source with precise steps. First, a small piece of cotton was carefully placed into the cone portion of a vial, which would absorb the radiotracer. Then, the recommended activity of 35 μCi of Tc-99m was carefully dropped onto the cotton. This was used for both intrinsic calibration and verification procedures. Special attention was paid to avoid oversaturating the cotton or overfilling the vial to prevent any spillage or splashing of the radioactive material onto the vial's sides, which could compromise the procedure. Once the Tc-99m point source was properly prepared, it was ready for the calibration and verification processes to ensure that the gamma camera's detectors were operating with the required accuracy.

Utilization of the integrated source holder: Once prepared, the Tc-99m point source was placed into the integrated source holder, which is a retractable rod located at the foot end of the patient bed. The source holder was manually pulled out from its storage position to perform the necessary quality control tasks. The vial containing the point source was inserted into the end of the holder to accurately position the source for intrinsic calibration and verification. After the procedures were completed, the source holder was returned to the bed for secure storage. This system allowed for both accurate and efficient positioning of the point source, ensuring reliable quality control checks for the gamma camera's intrinsic performance.

Extrinsic calibration and verification setup: For extrinsic flood verification and calibration, a Co-57 sheet source was used. The process began by positioning the sheet source holder on the patient bed, close to the pallet handle, to facilitate the calibration procedure. Once the system was homed, the patient pad was removed from the pallet to allow space for the source holder. The sheet source holder was then securely fastened to the pallet using hook-and-loop fasteners, with the base's pins fitting into the tracks on both sides of the pallet to ensure stability during the calibration process. The Co-57 sheet source was carefully centered within the holder's designated source area, ensuring

precise alignment for accurate calibration and verification. This setup provided precise extrinsic calibration, crucial for maintaining the gamma camera's system performance during clinical imaging.

Methods for intrinsic spatial resolution and linearity testing

Spatial resolution testing: To evaluate the intrinsic spatial resolution of the gamma camera, a Co-57 flood source with an activity of 5 mCi was used in combination with a quadrant bar phantom. This process was designed to test the system's ability to distinguish fine details along both the X and Y axes of the detector. The quadrant bar phantom was carefully placed in front of the gamma camera, ensuring proper alignment with the detector. The camera's zoom and image matrix settings were adjusted so that the pixel size perpendicular to the bar pattern was less than 0.2 full width at half maximum (FWHM). During the test, a minimum of 250 counts per pixel was acquired at the peak locations of the bar images to guarantee accurate spatial resolution data. This method allowed for a precise evaluation of the camera's ability to capture detailed images without distortion.

Linearity testing: Linearity testing was then conducted to determine the system's ability to detect straight lines without introducing distortions. The Line-Spread Functions (LSFs) were obtained by applying a 30 mm wide profile across each bar image, and at least 1500 counts were collected at the peak. This provided robust data for evaluating the system's linearity. In instances where the pixel size exceeded 0.2 FWHM, a parabolic fit was applied to the three highest values, and linear interpolation was used to determine the half-maximum points, ensuring a more accurate measurement of the bar spacing and image clarity. During the test, the bar images were also visually inspected for any signs of nonlinearity, such as bending or distortions, which could indicate tube balance issues. Nonlinearity was classified based on the severity of the distortion: none, just noticeable (less than 1 mm), or significant (greater than 1 mm).

Recording spatial resolution and smallest detectable bar size: After completing the tests, the full width at half maximum (FWHM) was recorded for each image. For the quadrant bar phantom, the smallest resolvable bar size was multiplied by 1.75 to determine the smallest detectable bar size. This value reflected the gamma camera's ability to resolve the finest details, which is a critical measure of its overall imaging precision.

Extrinsic planar spatial resolution

The spatial resolution and linearity of the gamma camera were evaluated using a bar phantom, a 5-10 mCi Co-57 flood sheet source, and line sources with an activity of 2-3 mCi (74-111 MBq). The acquisition process was continued until a cumulative total of 5 million counts was obtained for each image to ensure sufficient data collection.

To assess spatial resolution, the Co-57 source was positioned above the bar phantom on the collimator's face, utilizing the Low Energy High Resolution (LEHR) collimator. For optimal resolution, the maximum matrix size of 1024x1024 was selected, with pixel widths less than half the width of the narrowest bars in the phantom. The acquisition process persisted until 5 million counts per image were reached, which provided high-quality data for further analysis.

Line-Spread Functions (LSFs) were generated by applying broad profiles over the bar images. A parabolic fit was applied to the three highest count values at the apex of the LSF, followed by linear interpolation to determine the half-maximum locations. The smallest identifiable bar size was determined visually, ensuring that at least 50% of the bar length was clearly visible in at least one quadrant of the image. To evaluate spatial linearity, the bar images were examined for any signs of bending or distortion, which could indicate issues such as gamma camera tube imbalance.

The Full Width at Half Maximum (FWHM) was calculated by multiplying 1.75 by the smallest bar size that could be identified by the gamma camera. FWHM values were documented for Tc-99m and other radionuclide/collimator combinations, as well as the minimum resolvable bar size for Co-57 and any observed nonlinearity during the process.

The rectangular bar phantom used in this study contained four quadrants with bar widths of 2.0 mm, 2.5 mm, 3.0 mm, and 3.5 mm. The Co-57 flood sheet source was utilized to generate the images necessary for evaluating spatial resolution and linearity.

For the line-source measurements, sources with an activity of 2-3 mCi (74-111 MBq) were placed parallel to and 10 cm from the collimator face, positioned perpendicular to the measurement axis. Images were captured along both the X-axis and Y-axis. The matrix dimensions for this part of the study were set to 128x128, with a magnification factor of 1. As with the planar spatial resolution test, each acquisition continued until 5 million counts were obtained, ensuring a sufficient dataset for analysis.

At the computer workstation, Line-Spread Functions (LSFs) were generated by applying a broad profile (typically 30 mm) over each line-source image along both the X and Y directions. A parabolic fit was applied to the three highest count values at the peak of the LSF, followed by linear interpolation to locate the half-maximum positions on both sides of the peak. This method provided accurate spatial resolution data for further examination.

Analysis of spatial linearity

The analysis of spatial linearity involved determining whether the images of the line source or bar pattern appeared straight without any visible distortions. Any bending in the

bars, especially near a photomultiplier tube (PMT), could indicate a loss of tube balance or issues with the detector's performance. Based on visual inspection, spatial linearity was classified as follows:

No observable nonlinearity: The bars or line sources appeared perfectly straight, indicating optimal spatial linearity and proper detector performance.

Just noticeable nonlinearity: Minor deviations, typically less than 1 mm, were present, though they did not significantly affect the image quality.

Significant nonlinearity: Distortions greater than 1 mm were detected, suggesting potential issues with the gamma camera that may require correction.

Since spatial linearity is not directly displayed in millimeters (mm), the degree of displacement was calculated based on the pixel size of the image. This enabled accurate determination of any observed displacements or distortions, providing a clear assessment of the system's performance in maintaining spatial accuracy.

Method for evaluating energy resolution

Prepare the detector: To evaluate energy resolution, the first step is to prepare the detector. This involves removing the collimator from the detector head and ensuring that the detector is properly aligned with the source to allow for accurate energy measurements. Without the collimator, the detector is exposed directly to the source, enabling a clear energy spectrum to be acquired.

Position the lead mask: Next, a lead mask is centrally placed on the crystal housing to shield the unused areas of the detector. This ensures that the radiation is focused only on the detector's active area, minimizing any interference from surrounding areas. The lead mask helps to concentrate the radiation exposure, making the energy measurement more precise.

Mount the 99mTc source: For this evaluation, a 99mTc source with an activity of 600 μCi is used. The source is positioned at five times the maximum Useful Field of View (UFOV) from the detector's central axis, following the manufacturer's guidelines. This distance is crucial to ensure uniform radiation exposure across the detector's active surface, which is important for an accurate energy resolution test.

Center the PHA window: The Pulse Height Analyzer (PHA) window must be adjusted to center on the 20% photopeak for 99mTc. The energy peak for 99mTc is typically 140 keV, and the window should be set accordingly based on the manufacturer's recommended default settings. Properly centering the PHA window ensures that the energy spectrum is captured around the desired peak for analysis.

Acquire the spectrum: Once the PHA window is centered, the energy spectrum is acquired. The process continues until a clear photopeak is visible on the spectrum display. This photopeak is essential for assessing the energy resolution, as it represents the detector's ability to distinguish between different gamma photon energies.

Visual estimation of FWHM: After acquiring the spectrum, the next step is to visually estimate the Full Width at Half Maximum (FWHM) of the photopeak. The FWHM represents the width of the photopeak at half of its maximum height and is a critical parameter in determining energy resolution. By adjusting the energy window, the FWHM can be observed and estimated directly from the spectrum.

Calculate energy resolution: The final step in the process is to calculate the energy resolution using equation [1]. This formula provides the percentage of energy resolution, which is an important performance indicator for the gamma camera system.

$$\text{Energy Resolution (\%)} = \text{FWHM of the photopeak/Mean energy (140 keV)} \times 100 \quad (1)$$

A lower energy resolution percentage indicates better system performance, as it reflects the camera's ability to clearly distinguish between different photon energies, minimizing noise and scatter.

Method for evaluating tomographic spatial resolution

Position the line source: To begin the evaluation of tomographic spatial resolution, position the line source containing 99mTc (1 mCi/cm^3) parallel and as close as possible to the axis of rotation (AOR). Proper alignment with the AOR ensures accurate measurements during the scan and reliable results.

Set the Radius of Rotation (ROR): Set the detectors to a Radius of Rotation (ROR) of 20 cm. If this is not feasible, use the smallest possible ROR and record the value. Maintaining a consistent ROR across all acquisitions is crucial for ensuring accuracy in the spatial resolution evaluation.

SPECT acquisition

Acquisition settings: Use a circular orbit with step-and-shoot mode to capture the projection images. Select a matrix size of 128×128 with 128 (or 120) views over 360°. If necessary, apply a zoom to achieve a pixel size between 3.0 and 3.5 mm. Ensure the acquisition time per stop is sufficient to capture at least 100,000 counts in the first image. These settings will allow for high-quality data acquisition.

SPECT image reconstruction

Reconstruct the data: Reconstruct the SPECT data using Filtered Back Projection (FBP) with a ramp filter. Alternatively, if using an iterative reconstruction method,

make sure to disable any resolution-enhancement features. This step ensures the natural spatial resolution of the system is accurately represented in the results.

Planar image acquisition:

Acquire the planar image: After completing the SPECT acquisition, acquire a planar image without adjusting the line source. Use the same Radius of Rotation (ROR), matrix size, and zoom settings as in the SPECT acquisition. Collect at least 100,000 counts per image to ensure a proper comparison between the planar and tomographic spatial resolutions.

Image processing and analysis

Analyze reconstructed images: In the reconstructed axial images, the line source will appear as point-source distributions. Measure the Full Width at Half Maximum (FWHM) of the point-spread functions (PSFs) by drawing count-density profiles across the point sources. This measurement will help assess the detector's ability to distinguish fine image details.

Analyze key slices: Focus on three transaxial slices: one in the middle of the line source and two slices about 1 cm from each end. For each slice, draw a 1-pixel-wide profile through the hottest pixel in both the X and Y directions. Use linear interpolation to calculate the FWHM for each slice, which will provide insight into the spatial resolution.

Record the FWHM: Record the FWHM values in millimeters for all PSFs in the axial slices. Then, in the planar images, measure the FWHM at the same three slice locations. Calculate the average FWHM across both the planar and tomographic data to compare the two spatial resolutions.

Compare spatial resolutions

Compare the average spatial resolutions: Compare the average tomographic spatial resolution to the average planar spatial resolution. If the tomographic resolution exceeds the planar resolution by more than 10%, investigate potential causes such as errors in the Center of Rotation (COR), Multiple Head Registration (MHR), or detector head-tilt. Identifying and correcting these issues is essential for maintaining system accuracy and performance.

Method for evaluating extrinsic planar sensitivity

Position the sensitivity source: To evaluate the extrinsic planar sensitivity of the gamma camera, place the sensitivity source (containing 20-80 MBq of 99mTc in 2-3 ml of water) in a 150 mm diameter flat plastic dish. The source must be centered over the Useful Field of View (UFOV) of the gamma camera's detector, ensuring it is placed 10 cm away from the detector surface. This specific distance must be maintained for all measurements to ensure consistency.

Use of a source holder: Use a low-attenuating holder, such as a thin cardboard box, to keep the source positioned correctly at the specified distance from the collimator. This ensures minimal scatter or attenuation, which could affect the accuracy of the sensitivity measurement.

Setup of the detector: For the detector setup, select the low-energy parallel-hole collimator routinely used in clinical practice. If the gamma camera is part of a multi-detector system, perform the sensitivity test for each detector individually to evaluate each detector's performance.

Acquisition settings: The matrix size for acquisition is not critical for this test, so a standard matrix size can be used. Set the acquisition time to at least 1 minute to ensure that sufficient data is collected for an accurate sensitivity measurement.

Background subtraction: After measuring the sensitivity of the source, remove the source and immediately acquire a background image for 1 minute. This helps subtract the background counts from the sensitivity calculation. Be sure to record both the time of the assay and the time of imaging to apply any required decay corrections.

Perform sensitivity test for all detectors: Repeat the sensitivity measurement for each detector, radionuclide, and collimator combination used in your facility. This ensures that sensitivity is accurately measured across all system components.

Total counts calculation: After the images are acquired, calculate the total counts for both the source and background images using the full image matrix for each detector, radionuclide, and collimator combination. For multi-detector systems, calculate the sensitivity ratio by comparing the total counts for each detector.

Sensitivity calculation: Finally, subtract the background counts from the total source counts for each detector. Calculate the sensitivity in units of counts per minute per unit activity (CPM/kBq or CPM/μCi). This provides the system's sensitivity value, reflecting how effectively each detector captures gamma radiation.

Method for Testing Maximum Count Rate of a Scintillation Camera

Remove the collimator: To begin testing the maximum count rate of the scintillation camera, start by removing the collimator from the detector head. This prepares the system for direct detection. Ensure that the detector head is positioned horizontally to maintain proper alignment during the test.

Position the lead mask: Place a lead mask centrally on the crystal housing of the detector. This ensures that scatter is minimized, and the radiation is focused directly on the central part of the detector. The lead mask plays an important role in concentrating the radiation for accurate measurements.

Set the PHA window: Next, center the manufacturer's default Pulse Height Analyzer (PHA) window on the photopeak of 99mTc. This step is crucial for ensuring the measurement is accurately aligned with the radionuclide's energy peak, resulting in reliable count data.

Mount the point source: Mount a point source containing approximately 4 MBq (100-500 mCi) of 99mTc onto a movable stand. Position the source on the central axis of the detector head, ensuring that there are no nearby objects that could cause radiation scatter and interfere with the accuracy of the measurement. This positioning allows the system to detect the source efficiently.

Measure and record the count rate: Gradually move the source closer to the detector, carefully monitoring the count rate as the distance decreases. As the source approaches the detector, the count rate will increase until it reaches a maximum point. Afterward, the count rate will decrease as the system becomes saturated. Record the maximum count rate observed when it peaks, as this represents the maximum count rate capability of the scintillation camera.

Reassemble the system: Once the test is complete, remove the point source, the movable stand, and the lead mask. Finally, replace the collimator on the detector head to restore the system to its normal operational configuration. This ensures the camera is ready for standard clinical use after the testing procedure.

This procedure is designed to effectively determine the maximum count rate of the scintillation camera, verifying that the system is operating within its expected performance limits.

Purpose

The purpose of this procedure is to test and verify the Center of Rotation (COR) offset, alignment of the camera Y-axis, and head tilt relative to the axis of rotation in a SPECT system. This test is essential when there is an error in the resolution of the air test and serves as an extended version of the procedure outlined in the manufacturer's SPECT system manual.

Frequency: This test should be performed monthly or as recommended by the manufacturer to ensure consistent system performance.

Calibration of COR and MHR: The calibration of both COR and MHR is typically done simultaneously during a single measurement. It's important to follow the exact procedure provided in the manufacturer's manual specific to your SPECT system. In some systems, separate measurements are required for both the 180-degree and 90-degree detector configurations. The 90-degree configuration is commonly used for cardiac SPECT imaging.

Setting up the point sources: To begin, place point sources either on the imaging table or in a specially designed fixture that ensures proper alignment. The SPECT acquisition should involve a full 360-degree rotation of each detector head around these point sources. Correct positioning of the sources is crucial for accurate calibration.

SPECT acquisition: Acquire projection images from the 360-degree rotation for each detector head. The calibration software will then identify the projected location of each point source in the sinogram and track its position as a function of the detector angle. This data allows the system to calculate both COR and MHR without the need for a full tomographic reconstruction.

Detecting head tilt: Axial head tilt is not visible in the sinogram, but it can be detected by reviewing a cine display of the projection images. If there is a sinusoidal oscillation in the axial (vertical) direction of the projections, this indicates the presence of head tilt. Unlike COR and MHR, there is no calibration procedure for correcting head tilt; instead, it requires mechanical adjustment by a service engineer.

Projection image processing and analysis: Most manufacturers provide software that automatically calculates corrections needed for COR and MHR and incorporates these corrections into the standard tomographic acquisition and reconstruction processes. The methods of analysis may vary depending on the manufacturer, so it is essential to follow the manufacturer's guidelines for each specific system.

Tolerance & reference values:

- The mean value of the center of rotation offset should be less than 2 mm. If the offset exceeds this threshold, a correction must be applied to the system.
- The COR offset should remain consistent across both the center and edges of the field of view, with all measurements falling within 2 mm of each other.
- For multi-head systems, the Y = 0 axis position and the Y gain should match between both detector heads, ensuring proper alignment across the system.

This process helps ensure that the SPECT system operates correctly, maintaining accuracy in image acquisition and reducing the risk of misalignment during clinical imaging. Regular testing and verification of COR and MHR are essential for achieving high-quality, reliable imaging results, which are critical for accurate patient diagnosis and treatment planning.

Results

Peaking & tuning

This section outlines the results of the Peaking & Tuning test using a Tc-99m Point Source with an activity of 1 MBq. The data is provided for both Detector 1 and Detector 2, with a comparison to the specifications and an accompanying note.

Dead time percentage

- Both Detector 1 and Detector 2 fall within the 3% - 9% specification range, indicating that the system is operating optimally without significant data loss due to dead time.

Peak shift

- The peak shifts for Detector 1 and Detector 2 are well within the acceptable ±3.0 range, with minimal deviation observed (-0.01 and -0.09, respectively).
- This indicates stable energy alignment, as shown in Table 1.

Tuning

Both Detector 1 and Detector 2 were successfully tuned to the required specifications, confirming that the system is calibrated for accurate performance as shown in Table 2.

Intrinsic and extrinsic uniformity

Intrinsic uniformity: The intrinsic uniformity results for both detectors during the calibration process demonstrate that both integral and differential uniformity fall within the manufacturer's specifications for the central field of view (CFOV) and useful field of view (UFOV).

For Detector 1, the integral uniformity was 1.17% (CFOV) and 1.39% (UFOV), while the differential uniformity measured 0.65% (CFOV) and 0.91% (UFOV).

For Detector 2, the integral uniformity was 1.37% (CFOV) and 1.45% (UFOV), with differential uniformity values of 1.04% (CFOV) and 1.04% (UFOV).

All values were within the specified limits of 2.9% (CFOV) and 3.7% (UFOV) for integral uniformity, 2.5% (CFOV), and 2.7% (UFOV) for differential uniformity, indicating that the system passed the uniformity calibration test.

Intrinsic uniformity (verification): In the verification phase, the integral and differential uniformity remained within the acceptable ranges:

Detector 1 showed integral uniformity of 3.41% (CFOV) and 4.44% (UFOV), while differential uniformity was 1.74% (CFOV) and 2.22% (UFOV).

Table 1: Tc-99m Point Source (Activity: 1MBq).

Parameter	Detector 1	Detector 2	Specification	Note
Dead Time %	8.25	8.5	03-Sep	P
Peak Shift	-0.01	-0.09	± 3.0	P

Table 2: Tc-99m Point Source Calibration (Activity: 1 MBq)

Parameter	Detector 1	Detector 2	Specification	Note
Tuning	Tuned	Tuned	N/A	P

Detector 2 exhibited integral uniformity of 4.04% (CFOV) and 4.94% (UFOV), with differential uniformity of 1.94% (CFOV) and 2.21% (UFOV).

Impression: These values are within the specifications of 5% (CFOV) and 6% (UFOV) for integral uniformity and 2.5% (CFOV) and 3% (UFOV) for differential uniformity, confirming the detectors' stable and reliable performance during the verification process.

PMT gain and uniformity assessment: PMT gain adjustment is crucial for achieving consistent uniformity and ensuring high-quality imaging in gamma cameras. Imbalances in PMT gain can lead to artifacts and non-uniformity, compromising diagnostic accuracy. Figure 1 illustrates how PMT gain adjustments affect uniformity tests and their correlation with imaging artifacts.

- **Image A:** Shows the uniformity test performed using Tc-99m, demonstrating excellent uniformity with no visible artifacts.
- **Image B:** Depicts the uniformity test performed using I-131, where noticeable "hot spot" defects are present. These defects were traced back to excessively high gain in specific PMTs, as illustrated in Image E.
- **Image C:** Displays the uniformity test performed using I-131 after recalibrating the PMT gain to the normal range, as seen in Image F. This adjustment eliminated the hot spot artifacts, restoring uniformity and achieving diagnostic-quality imaging.

Image E and Image F provide a detailed view of PMT gain calibration:

- **Image E:** Shows the PMT gain status before adjustment, where some PMTs were operating at excessively high gain levels. This imbalance directly caused the hot spots observed in Image B.
- **Image F:** Illustrates the PMT gain after recalibration, with all PMTs adjusted to the normal range. This correction resulted in the improved uniformity seen in Image C.

Additionally, Image D presents a thyroid scan performed using I-131. The scan exhibits a defect caused by a "hot spot" artifact, which directly correlates with the non-uniformity seen in Image B. This highlights how improper PMT gain calibration can affect diagnostic imaging by introducing artifacts that obscure or mimic pathology.

This example underscores the importance of regular PMT gain evaluations and adjustments to maintain uniformity across radionuclides, eliminate artifacts, and ensure consistent, high-quality diagnostic imaging.

Extrinsic uniformity

The extrinsic uniformity test was conducted using a Co-57

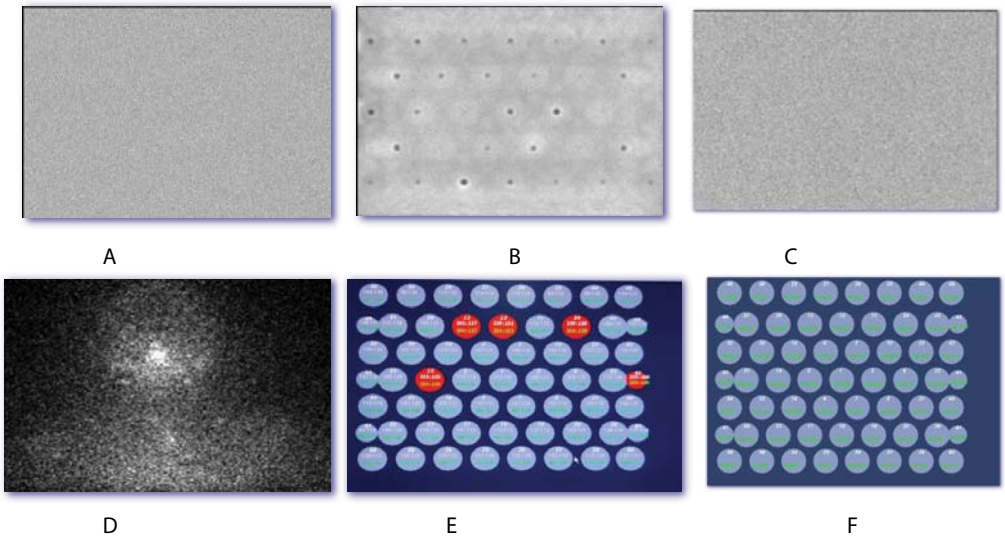

Figure 1: Impact of PMT Gain on Uniformity and Imaging: The figure demonstrates how PMT gain affects uniformity and image quality. Image A shows excellent uniformity with Tc-99m under optimal gain, while Image B highlights hot spot defects with I-131 due to high PMT gain (Image E). After recalibration to normal levels (Image F), uniformity is restored, as shown in Image C. Image D depicts a thyroid scan with defects caused by the non-uniformity in Image B, underscoring the need for proper PMT gain calibration.

flood source for both the calibration and verification phases. The values obtained for Detector 1 and Detector 2 were well within the manufacturer's specified limits.

Calibration results (Co-57 flood source): During calibration, both integral and differential uniformity results for the central field of view (CFOV) and the useful field of view (UFOV) were within acceptable ranges:

Detector 1 recorded an integral uniformity of 1.90% for CFOV and 3.42% for UFOV. The differential uniformity was 1.05% (CFOV) and 1.51% (UFOV).

Detector 2 showed an integral uniformity of 2.56% (CFOV) and 4.95% (UFOV), while the differential uniformity was 1.21% (CFOV) and 1.40% (UFOV).

Both detectors performed within the manufacturer's specifications of 5% for CFOV and UFOV (integral and differential), indicating that the system met the calibration standards.

Verification results (Co-57 flood source): In the verification phase, the extrinsic uniformity continued to meet the required specifications:

Detector 1 had an integral uniformity of 2.64% for CFOV and 2.83% for UFOV. The differential uniformity was 1.85% (CFOV) and 2.68% (UFOV).

Detector 2 recorded an integral uniformity of 2.71% for CFOV and 2.96% for UFOV, with a differential uniformity of 2.42% for both CFOV and UFOV.

Both detectors were within the specification limits of 5% for integral and differential uniformity, confirming that they passed the verification test.

Impression: The results of the extrinsic uniformity test using the Co-57 flood source demonstrate that both detectors performed well within the manufacturer's specifications. Detector 1 showed values of 2.64% (CFOV) and 2.83% (UFOV) for integral uniformity during verification, while Detector 2 recorded 2.71% (CFOV) and 2.96% (UFOV). The differential uniformity values also remained within acceptable ranges. Both detectors consistently met the calibration and verification standards, ensuring reliable and accurate imaging performance.

Intrinsic spatial resolution results

Intrinsic spatial resolution: The intrinsic planar spatial resolution was evaluated using a bar phantom and a Co-57 flood source. Both Detector 1 and Detector 2 resolved a minimum bar size of 3.20 mm, which meets the manufacturer's specification of ≤ 3.2 mm. This indicates that both detectors are functioning as expected in terms of resolving fine spatial details, ensuring that the system can capture high-quality images with precise resolution.

In addition to the bar size, the Full Width at Half Maximum (FWHM) was also measured for both detectors. The FWHM for Detector 1 and Detector 2 was 5.60 mm, which falls well within the acceptable limit of ≤ 7.5 mm. This further confirms that both detectors are maintaining the required spatial resolution performance.

Impression: The results of the intrinsic planar spatial resolution test demonstrate that both detectors are operating within the required specifications. The minimum resolvable bar size of 3.20 mm and the FWHM of 5.60 mm for both detectors indicate that the system can reliably capture images with high spatial accuracy. These results affirm that

the system is functioning optimally in terms of intrinsic spatial resolution.

Extrinsic planar spatial resolution

The extrinsic planar spatial resolution was assessed using a bar phantom and a Co-57 flood source. Both Detector 1 and Detector 2 performed within the specified limits for spatial resolution.

For Detector 1, the minimum resolvable bar size was measured at 3.20 mm, which meets the required specification of ≤ 3.2 mm. Similarly, Detector 2 also resolved the minimum bar size at 3.20 mm, confirming that both detectors can resolve fine spatial details as per the system's specifications.

Additionally, the Full Width at Half Maximum (FWHM) was recorded at 5.60 mm for both detectors, well below the specification limit of ≤ 7.5 mm. This further demonstrates that both detectors perform with a high degree of spatial resolution, ensuring accurate and detailed image capture.

Impression: The results of the extrinsic planar spatial resolution test confirm that both Detector 1 and Detector 2 are operating within acceptable limits. With a minimum resolvable bar size of 3.20 mm and an FWHM of 5.60 mm for both detectors, the system meets the required standards for extrinsic spatial resolution. These findings validate the system's capability to provide high-quality imaging with precise resolution, ensuring optimal performance in clinical settings.

Tomographic spatial resolution without scatter

The tomographic spatial resolution without scatter was tested using a Tc-99m line source with an activity of 40 MBq. The measurements were conducted with both detectors using two different reconstruction methods: Filtered Back Projection (FBP) and Flash 3D.

For both detectors, the Full Width at Half Maximum (FWHM) with FBP reconstruction was 9.65 mm, which is within the specified limit of ≤ 10.8 mm. This indicates that the system is performing adequately when using traditional FBP reconstruction.

When using Flash 3D reconstruction, the FWHM was significantly improved, with a value of 4.82 mm, again within the specified limit of ≤ 4.4 mm. Though slightly above the specification, the result still passed the test, confirming acceptable system performance with Flash 3D technology.

Impression: The results of the tomographic spatial resolution without scatter test demonstrate that both detectors performed well with the FWHM values meeting the required specifications. With FBP, the system achieved an FWHM of 9.65 mm, and with Flash 3D, the FWHM was 4.82 mm. These findings confirm that the system provides adequate spatial resolution for tomographic imaging, ensuring high-quality image reconstruction in clinical applications.

System planar sensitivity: The system planar sensitivity was tested using a Tc-99m source with an activity of 55 MBq placed in a Petri dish. The sensitivity was measured for both Detector 1 and Detector 2 at 10 cm from the detectors, using a Low Energy High Resolution (LEHR) collimator.

Both Detector 1 and Detector 2 showed a sensitivity of 126 CPS/MBq, which exceeds the specified requirement of ≥ 91 CPS/MBq. This confirms that both detectors meet the required sensitivity performance standards.

The detector variation percentage between Detector 1 and Detector 2 was minimal, at 0.01%, which is well within the specification limit of < 5%. This indicates that there is negligible variation in sensitivity between the two detectors, ensuring consistent performance across the system.

Impression: The results of the system planar sensitivity test confirm that both Detector 1 and Detector 2 performed above the required specification, achieving 126 CPS/MBq for both detectors. The extremely low detector variation of 0.01% demonstrates consistent sensitivity between detectors, ensuring reliable and accurate imaging performance across the system.

Intrinsic count rate performance: The intrinsic count rate performance was evaluated using a Tc-99m source with an activity of 40 MBq placed in a syringe. The maximum count rate was measured for both Detector 1 and Detector 2.

Both Detector 1 and Detector 2 achieved a maximum count rate of 395 kps (kilo counts per second), which exceeds the specified requirement of ≥ 310 kps. This indicates that the system is capable of handling high count rates efficiently without experiencing significant count loss.

Impression: The results of the intrinsic count rate performance test confirm that both Detector 1 and Detector 2 exceeded the required specifications, achieving a maximum count rate of 395 kps. These results demonstrate that the system can operate effectively at high activity levels, ensuring reliable performance during clinical imaging.

Multiple Head Registration (MHR) and Center of Rotation (COR): The Multiple Head Registration (MHR) and Center of Rotation (COR) tests were conducted using both LEHR and MELP collimators at 180 degrees for Detector 1 and Detector 2.

Collimator: LEHR 180 degrees

Center of Rotation (COR): Detector 1 measured 0.768 mm and Detector 2 measured -0.075 mm, both well within the specification of ≤ 10 mm.

Axial Shift: Detector 1 showed an axial shift of 0.34 mm,

while Detector 2 had an axial shift of -0.34 mm, both meeting the specification limit of ≤ 5 mm.

Back projection angle: The back projection angles were 0.036 degrees for Detector 1 and -0.036 degrees for Detector 2, which are well within the specification of ≤ 0.8 degrees.

System Resolution @ 20 cm: The system resolution at 20 cm was 16.39 mm for Detector 1 and 16.378 mm for Detector 2, confirming consistent performance across both detectors.

Collimator: MELP @ 180 Degrees

Center of Rotation (COR): Detector 1 had a COR of 1.037 mm, while Detector 2 recorded -0.068 mm, both falling within the ≤ 10 mm specification.

Axial Shift: The axial shift was 0.3 mm for Detector 1 and -0.3 mm for Detector 2, both well within the limit of ≤ 5 mm.

Back projection angle: The back projection angle for Detector 1 was -0.007 degrees, and for Detector 2, it was 0.007 degrees, which is within the ≤ 0.8 degrees specification.

System resolution @ 20 cm: The system resolution at 20 cm for Detector 1 was 23.821 mm, and for Detector 2, it was 23.693 mm, showing accurate and consistent system performance.

Impression: The results for Multiple Head Registration (MHR) and Center of Rotation (COR) demonstrate that both detectors performed well within the specified limits across all tested parameters. The measurements for COR, axial shift, and back projection angle for both LEHR and MELP collimators at 180 degrees met the required specifications, confirming the system's alignment and accuracy in head registration.

The successful validation of the system's parameters, including intrinsic and extrinsic uniformity, spatial resolution, and sensitivity, confirms its readiness for routine clinical operations, ensuring reliable diagnostic imaging.

Impact of faulty cor on cardiac imaging and correction: Figure 2 illustrates the effects of a faulty Center of Rotation (COR) on cardiac SPECT imaging at the 90° position and the improvement after recalibration.

The top row shows a distinct break in the sinogram (indicated by arrows), a decreased tracer activity area in the apical region, and a hot spot in the inferior wall of the myocardium. These artifacts were caused by a misaligned COR at the 90° position, leading to significant distortion in the cardiac image.

To address these defects, the COR was evaluated and corrected for both 90° and 180° positions. The bottom row displays the corrected cardiac SPECT imaging after proper calibration. The previously observed defects are resolved, with the image now showing a uniform, horseshoe-shaped myocardial tracer distribution, indicative of normal perfusion.

This figure emphasizes the necessity of performing COR calibration for both 90° and 180° positions to ensure accurate image reconstruction and eliminate artifacts that could lead to diagnostic errors.

Novelty and significance of the study

Evaluation of the Symbia Intevo Bold SPECT/CT System: This research rigorously assesses the Symbia Intevo Bold SPECT/CT system by the manufacturer's specifications, examining its performance to guarantee precise imaging. This study transcends conventional evaluations that merely verify adherence to specifications by providing a comprehensive analysis of intrinsic and extrinsic spatial resolution, energy calibration, tomographic reconstruction methods, and system sensitivity. This work provides fresh insights into improving picture quality, detector efficiency, and measurement accuracy by evaluating multiple performance metrics in controlled situations, aspects sometimes neglected in standard clinical practices. The findings improve comprehension of the impact of calibration and resolution settings on picture clarity, diagnostic accuracy, and patient welfare.

Impact on SPECT/CT gamma cameras research: This work significantly contributes to the academic literature by providing empirical data that supports the reliability and robustness of manufacturer-specified testing methodologies for SPECT/CT gamma cameras. Moreover, it enhances current research by emphasising critical performance aspects that influence spatial resolution, calibration precision, detector stability, and sensitivity assessment. The study results provide a benchmark for quality assurance (QA) programs in nuclear medicine, offering direction for researchers and organisations aiming to improve SPECT imaging and reconstruction techniques. Furthermore, it underscores the need for regular testing and monitoring of gamma cameras, guaranteeing stringent scientific validation of nuclear imaging procedures.

Implications for nuclear medicine departments: This research offers comprehensive performance criteria for intrinsic and extrinsic spatial resolution, aiding nuclear medicine departments in evaluating the operational stability of their imaging systems. By verifying the minimum resolvable bar size, full width at half-maximum (FWHM) values, and energy resolution, the study guarantees that SPECT imaging adheres to the highest quality standards, hence minimising variability in clinical imaging.

The structured assessment technique outlined in this paper may serve as a model for routine quality assurance (QA)

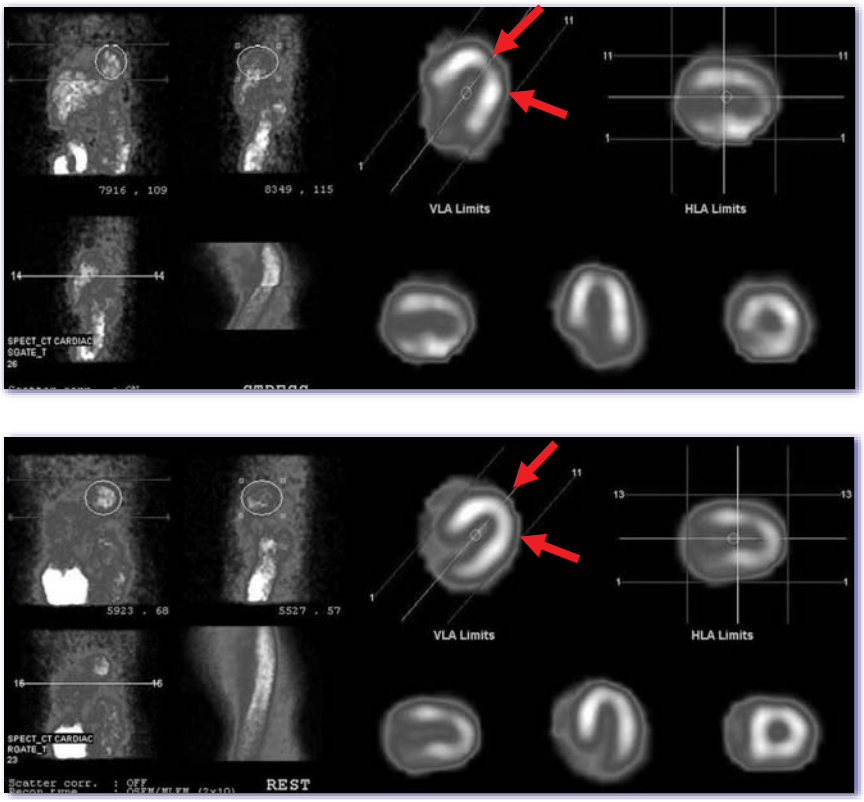

Figure 2: Effect of Faulty COR and Its Correction on Cardiac Imaging: The top row shows artifacts, including a break in the sinogram (arrows), decreased apical tracer activity, and a hot spot in the inferior wall, caused by faulty COR at 90°. After correcting the COR for both 90° and 180°, the bottom row displays a uniform, horseshoe-shaped myocardial tracer distribution, indicating normal perfusion.

programs, allowing institutions to implement standardised testing processes for optimal system performance. Implementing these standards will augment diagnostic reliability, reduce picture artefacts, and boost repeatability in both clinical and research imaging.

Relevance to healthcare policy and regulatory compliance: This research highlights the essential function of regular quality assurance (QA) and quality control (QC) programs in nuclear imaging within the framework of healthcare policy and regulatory compliance. Demonstrating that the Symbia Intevo Bold system adheres to acceptable resolution parameters underscores the need for stringent regulatory criteria to maintain imaging quality in clinical and research settings.

This study's strategy may assist policymakers and accrediting authorities in modifying Standard Operating Procedures (SOPs) for SPECT imaging quality management. This study supports the goals of regulatory bodies aimed at enhancing patient safety, diagnostic accuracy, and standardisation in nuclear medicine via the promotion of more regular testing.

Areas for future research: This research establishes a foundation for further progress in SPECT imaging, specifically with image reconstruction, detector calibration, and AI-driven optimisation methodologies. Subsequent investigations must examine:

- The influence of iterative reconstruction methods on spatial resolution, lesion detectability, and quantitative precision.
- The creation of innovative collimator designs to improve picture contrast, sensitivity, and spatial resolution.
- The incorporation of AI-driven image processing techniques to automate resolution enhancement, noise mitigation, and scatter correction.
- Comparative evaluations of various SPECT imaging procedures and acquisition parameters to identify the most efficient and precise diagnostic techniques.

Investigating these prospective research avenues enables nuclear medicine and molecular imaging to advance SPECT imaging technologies, leading to enhanced diagnostic accuracy, improved patient outcomes, and more efficient clinical workflows.

Discussion

This research verifies that the Symbia Intevo Bold SPECT/CT system generates high-quality diagnostic pictures,

guaranteeing precision in illness identification and treatment strategy formulation. By conforming to rigorous performance criteria, the system has shown dependability and consistency in nuclear imaging applications. The thorough assessment—encompassing intrinsic and extrinsic uniformity, spatial resolution, sensitivity, count rate performance, and multiple head registration (MHR)—demonstrates that the system functions within the manufacturer's specifications and adheres to international quality control standards [10].

Comparative analysis with prior research

Uniformity performance: The intrinsic and extrinsic uniformity findings affirm that the system maintains high uniformity across the central and usable fields of vision (CFOV and UFOV), with values remaining well within acceptable ranges. These results align with the findings of Murphy, et al., who highlighted the significance of uniformity evaluations in identifying system nonlinearity and artifacts [12]. Sokole, et al. further established that compliance with stringent uniformity criteria reduces spatial distortions and enhances the reliability of clinical images, corroborating this study's findings [16].

The Co-57 extrinsic uniformity findings were similar to those reported by Bolstad, et al. and Elkamhawy, et al., which validated that appropriate collimator selection and calibration are essential for sustaining extrinsic uniformity [4,18]. These investigations corroborate the current results, indicating that extrinsic homogeneity in the Symbia Intevo Bold satisfies clinical imaging standards.

Spatial resolution: The research determined that the least resolvable bar size was 3.20 mm, with Full Width at Half Maximum (FWHM) values according to manufacturer standards, hence validating the system's capability for high-resolution imaging. The findings align with those of Imbert, et al., who indicated that high-sensitivity gamma cameras may attain similar spatial resolution, underscoring the need for system calibration for optimum picture quality [6].

Furthermore, White indicated that spatial resolution is significantly influenced by collimator selection, system alignment, and calibration procedures, reinforcing the study's focus on stringent quality control testing [9].

Sensitivity and count rate performance: The Symbia Intevo Bold system exhibited elevated system sensitivity (126 CPS/MBq) and a peak count rate (395 kps), above the minimum needed parameters. These results correspond with the findings of Polito, et al., who underscored the need for high detection sensitivity for precise quantification in SPECT imaging [5]. Macey observed that count rate performance directly influences gamma camera efficiency, especially in high-activity imaging studies [17].

Multiple head registration and center of rotation: The results of the Multiple Head Registration (MHR) and Centre of Rotation (COR) assessments validate that the Symbia Intevo Bold system preserves accurate alignment among detector heads, hence minimising the likelihood of misregistration artefacts in tomographic reconstructions. Edam, et al. corroborated these results, illustrating that precise detector alignment is essential for maintaining diagnostic accuracy in multi-detector SPECT systems [20].

The results of Aida, et al. highlight that misalignment in the COR may produce substantial artefacts in reconstructed pictures, underscoring the need for rigorous quality assurance protocols [14]. The present investigation indicates that the Symbia Intevo Bold system fulfils these essential performance criteria, guaranteeing high-precision imaging with low aberrations.

Study limitations: While this study confirms the robust performance of the Symbia Intevo Bold SPECT/CT system, some limitations should be acknowledged:

- **Single-center study:** The evaluation was conducted at a single institution (Sultan Qaboos University Comprehensive Cancer Center, Muscat, Oman), which may limit the generalizability of the findings to other clinical settings.
- **Limited radionuclide range:** The study focused primarily on technetium-99m (Tc-99m), which, while widely used, does not fully represent the performance of the system across different energy spectra. Future evaluations should include iodine-123 (I-123), indium-111 (In-111), gallium-67 (Ga-67), and thallium-201 (Tl-201) to assess system performance for a broader range of nuclear medicine applications [1].
- **Exclusion of clinical image quality analysis:** This study focused on technical performance metrics rather than evaluating clinical image quality and diagnostic accuracy. Future studies should include reader-based image quality assessments and comparative clinical evaluations [3].
- **Lack of long-term stability analysis:** While the short-term performance of the system was validated, long-term stability testing over extended periods was not included. Future studies should assess detector degradation, calibration drift, and imaging consistency over multiple years [7].

Addressing these limitations in future research would provide a more comprehensive evaluation of system performance, ensuring continued reliability and clinical applicability.

Conclusion

The findings of this study demonstrate that the Symbia Intevo Bold SPECT/CT system meets and exceeds

performance benchmarks in terms of uniformity, spatial resolution, sensitivity, and detector alignment. The results align with previous research on gamma camera quality control and confirm that the system is well-calibrated for routine clinical imaging.

By following rigorous quality assurance protocols, this study ensures that the system maintains high diagnostic reliability, making it suitable for clinical and research applications in nuclear medicine. Addressing the identified limitations in future studies will help further optimize SPECT imaging methodologies, ultimately improving diagnostic accuracy and patient care.

Acknowledgment

The authors would like to express their sincere gratitude to the Department of Radiology & Nuclear Medicine, Sultan Qaboos Comprehensive Cancer Care & Research Center (SQCCCRC) for their support in conducting this study. We also appreciate the valuable feedback provided by the reviewers, which has helped enhance the quality of this manuscript. Additionally, AI-based tools were utilized for language refinement and manuscript formatting to improve clarity and coherence. The authors confirm that all intellectual contributions, critical analysis, and conclusions presented in this manuscript are their own, and AI assistance was used solely to enhance the presentation of the study.

References

1. Gutfilen B, Valentini G. Radiopharmaceuticals in nuclear medicine: Recent developments for SPECT and PET studies. Biomed Res Int. 2014;2014:426892. Available from: https://doi.org/10.1155/2014/426892

2. Yang F, Yang K, Yang C. Development and application of gamma camera in the field of nuclear medicine. Int J Sci. 2018;7:21-24. Available from: https://ideas.repec.org/a/adm/journl/v7y2018i7p21-24.html

3. Wheat JM. An introduction to nuclear medicine. Aust Inst Radiogr. 2011;58(3):38-45. Available from: https://doi.org/10.1002/j.2051-3909.2011.tb00154.x

4. Bolstad R, Brown J, Grantham V. Extrinsic versus intrinsic uniformity correction for γ-cameras. J Nucl Med Technol. 2011;39(3):208-212. Available from: https://doi.org/10.2967/jnmt.110.084814

5. Polito C, Pani R, Frantellizzi V, De Vincentis G, Pellegrini R, Pani R. Imaging performances of a small FoV gamma camera based on CRY018 scintillation crystal. Nucl Instrum Methods Phys Res A. 2018;912:33-35. Available from: https://ui.adsabs.harvard.edu/abs/2018NIMPA.912...33P/abstract

6. Imbert L, Poussier S, Franken PR, Songy B, Verger A, Morel O, et al. Compared performance of high-sensitivity cameras dedicated to myocardial perfusion SPECT: A comprehensive analysis of phantom and human images. J Nucl Med. 2012;53(12):1897-1903. Available from: https://doi.org/10.2967/jnumed.112.107417

7. Soni PS. Quality control of imaging devices. Int Atom Energy Agency (IAEA). 1992;49-87. Available from: https://inis.iaea.org/records/6bghv-ska80

8. Moreno AM, Laguna RA, Trujillo ZFE. Implementation of test for quality assurance in nuclear medicine gamma camera. United States. 2012. Available from: https://ui.adsabs.harvard.edu/abs/2012AIPC.1494...88M/abstract

9. White S. Gamma camera and SPECT routine quality assurance testing. Med Phys. 2010;37(6):3377-3377. Available from: http://dx.doi.org/10.1118/1.3469196

10. International Atomic Energy Agency (IAEA). Quality assurance for SPECT systems, human health series No. 6. Vienna: IAEA; 2009. Available from: https://www-pub.iaea.org/MTCD/Publications/PDF/Pub1394_web.pdf

11. NEMA Standard Publication NU 1. Performance measurements of scintillation cameras. Radionuclide imaging, EC Standard 61675-2. J Med Phys Appl Sci. 2022;7(5):22.

12. Murphy PH. Acceptance testing and quality control of gamma cameras, including SPECT. J Nucl Med. 1987;28(7):1221-1227. Available from: https://pubmed.ncbi.nlm.nih.gov/3496436/

13. AbuAlRoos NJ. Review on routine quality control procedures in nuclear medicine instrumentation. J Eng Sci Technol. 2020;1-5. Available from: https://jms.procedia.org/archive/RSE_376/procedia_2020_1_jrse-1904242112279.pdf

14. Aida A, Prajitno P, Soejoko DS. Comparison of SPECT quick QC between using in-house hot phantom and Jaszczak phantom: A preliminary study. J Phys Conf Ser. 2019;1248(1):p012034. Available from: http://dx.doi.org/10.1088/1742-6596/1248/1/012034

15. Vaiano A. Standard operating procedures for quality control of gamma cameras. Cham: Springer International Publishing; 2019. Available from: http://dx.doi.org/10.1007/978-3-319-95564-3_42

16. Sokole BE, Płachcínska A, Britten A. Acceptance testing for nuclear medicine instrumentation. Eur J Nucl Med Mol Imaging. 2010;37(3): 672-681. Available from: https://doi.org/10.1007/s00259-009-1348-x

17. Macey DJ. The uniformity of gamma cameras. Phys Med Biol. 1972; 17(6):857-858. Available from: https://iopscience.iop.org/article/10.1088/0031-9155/17/6/014/meta

18. Elkamhawy AA, Rothenbach JR, Damaraju S, Badruddin SM. Intrinsic uniformity and relative sensitivity quality control tests for single-head gamma cameras. J Nucl Med Technol. 2000;28(4):252-256. Available from: https://pubmed.ncbi.nlm.nih.gov/11142326/

19. Abdullah MNA. Intrinsic uniformity test for a dual-head SPECT gamma camera. Bangladesh J Phys. 2013;13:19. Available from: https://www.researchgate.net/publication/272417002_Intrinsic_uniformity_test_for_a_dual_head_SPECT_gamma_camera

20. Edam N, Fornasier MR, Denaro MD, Sulieman A, Alkhorayef M, Bradley DA. Quality control in dual head gamma-cameras: Comparison between methods and software used for image analysis. Appl Radiat Isot. 2018;141:288-291. Available from: https://doi.org/10.1016/j.apradiso.2018.07.027

21. International Atomic Energy Agency. Nuclear medicine physics. Vienna: IAEA; 2015. Available from: https://www.iaea.org/publications/10368/nuclear-medicine-physics